

Journal of Mechanics of Materials and Structures

**ANALYTICAL SOLUTION FOR DUCTILE AND FRC PLATES ON ELASTIC
GROUND LOADED ON A SMALL CIRCULAR AREA**

Enrico Radi and Pietro Di Maida

Volume 9, No. 3

May 2014



ANALYTICAL SOLUTION FOR DUCTILE AND FRC PLATES ON ELASTIC GROUND LOADED ON A SMALL CIRCULAR AREA

ENRICO RADI AND PIETRO DI MAIDA

The problem of a large FRC slab resting on a Winkler-type elastic foundation and subject to a transversal load distributed over a small circular area is investigated in the present work. The mechanical behavior is described by the Kirchhoff theory of elastic-perfectly plastic plates obeying Johansen's yield criterion and associative flow rule. The governing equations within both the inner elastic-plastic circular region near to the loaded area and the outer elastic region are found in terms of the transversal displacement and solved in closed form, under the hypothesis of proportional loading. After the formation of positive yield lines, namely radial cracks at the bottom side of the plate, the onset of a negative yield line, namely a circumferential crack at the upper side of the, defines the load-carrying capacity of the slab on grade. Two possible configurations are envisaged, depending on whether the circumferential crack occurs within the inner elastic-plastic region, where radial cracks take place on the bottom side thus activating a plastic mechanism, or within the outer uncracked elastic region. The ratio between the subgrade modulus and flexural rigidity of the plate allows introducing a characteristic length. The influence of both material and geometrical parameters on the load-carrying capacity of the plate is then investigated. Based on the analytical results, a simplified method for the calculation of the load-carrying capacity of FRC slabs on grade is also proposed and compared with previously developed models.

1. Introduction

Concrete slabs on ground floor of factory buildings are designed to support heavy concentrated loads transmitted by columns, vehicle wheels and machinery arranged on them. To prevent cracking and collapse of concrete industrial floors, the introduction of steel reinforcement and/or welded wire meshes is a current practice. Alternatively, the addition of steel or polymeric fibers in the concrete mix may totally or partially substitute the steel reinforcement. The latter solution is becoming widely used in the construction of concrete slabs on grade, since it has proved to be efficient and cost-effective. Indeed, it can provide crack control for shrinkage and temperature effects. Moreover, it may improve the mechanical properties of concrete, as well as the flexural behavior and the fracture toughness of the slab, resulting in significant load-carrying capacity after the concrete has cracked [Falkner et al. 1995]. Full advantage of the addition of fibers to the concrete mix occurs for statically indeterminate structures, where plastic hinges and redistribution of stress take place. In particular, the post cracking capacity of the FRC slabs allows for a redistribution of moments after initial cracking, which let the FRC slab behave in a ductile manner thus increasing its carrying capacity [Barros and Figueiras 1998; 1999; 2001]. However, a valuable increase in the load-carrying capacity of the slab occurs only for a proper dosage of fibers.

Keywords: Kirchhoff plate theory, Winkler elastic subgrade, load-carrying capacity, yield lines, elastic-perfectly plastic material, Johansen's yield criterion, fiber reinforced concrete.

Indeed, the results of large scale load tests [Bischoff et al. 2003] predict that a low dosage of fibers provides little improvement when compared with unreinforced concrete slab and thus is not an effective substitute for welded wire reinforcement in slabs on grade.

Due to the damping effect of the soil out of the loaded region, the problem of a concentrated load acting on the top of a FRC slab on grade, or uniformly distributed over a small circular area, can be modeled by considering an infinitely large Kirchhoff plate resting on an elastic foundation. Within these assumptions, the elastic theory developed by Westergaard [1948] provides an approximate solution that is reliable for small loads only. Westergaard approach is also not suitable for FRC slabs because it does not take into account the post crack behavior. For a better evaluation of the load-carrying capacity of FRC slabs, the nonlinear behavior of fiber reinforced concrete must necessarily be taken into account. Following this approach, Meyerhof [1960; 1962] performed a limit analysis of the problem, by considering rigid-perfectly plastic behavior of the material. This author assumed that the slab is driven into the subgrade until a conical plastic mechanism develops in the slab, consisting of an infinite number of radial positive yield lines (centered fan) and an ultimate circumferential crack (i.e., a negative yield line), whose radius is determined in an approximate way. According to the upper-bound theorem of limit analysis, this kind of analysis should predict an upper bound to the collapse load, being performed under the assumption of a kinematically admissible collapse mechanism, which does not necessarily coincide with the effective one.

Generally, investigations based on the limit analysis theory [Meyerhof 1960; 1962; Gazetas and Tassios 1978; Losberg 1978, Baumann and Weisgerber 1983, Rao and Singh 1986] supply statically inadmissible distributions of bending moments and shear forces and/or introduce some degrees of arbitrariness in the choice of the plastic mechanism, e.g., in the radius of the circumferential crack and distribution of the subgrade reaction. Moreover, the limit analysis theory does not provide the plate deflection under the ultimate load. Later, the finite element method was employed by Shentu et al. [1997] in order to analyze the stress and deformation fields in concrete slabs on ground, by considering Ottosen's failure criterion. On the basis of these numerical investigations, a new analytical method was proposed [ibid.] for computing the ultimate load-carrying capacity of concrete slabs on ground. However, the model requires the measurement of the direct tensile strength of the concrete, which may introduce a high degree of uncertainty. Belenkiy [2007] proposed an application of the principle of stationary total energy in order to obtain an upper bound solution of bending problems for plates on elastic foundation.

A limited amount of work also exists on elastic-perfectly plastic plates on elastic foundations [Sokól-Supel 1985; 1988; Kocatürk 1997]. By extending the analysis developed by Tekinalp [1957] for a ductile plate under bending, Sokól-Supel performed analytical studies on the behavior of a metallic circular plate with clamped, hinged or free edge on a tensionless Winkler foundation under axisymmetric, statically increasing loading. In a preliminary work [Sokól-Supel 1985], the material is assumed to obey the Johansen's yield criterion with the associative flow rule. Then, a Tresca-type yield criterion is considered in a following study [Sokól-Supel 1988]. Later, the investigations have been extended to elastic-plastic subgrade under column load [Kocatürk 1997]. More general yielding criteria that can be adopted for concrete and FRC have been recently formulated by Bigoni and Piccolroaz [2004], Piccolroaz and Bigoni [2009] and Poltronieri et al. [2014]. These elastic-plastic constitutive models may correctly represent triaxial test results at high confining pressure and thus they can be efficiently adopted to describe the stress state arising under and in proximity of the loaded region.

A refined analytical investigation of the load-carrying capacity for a large FRC slabs on grade loaded on a small internal area is presented here. The model assumes elastic-perfectly plastic behavior of the material in order to simulate the post cracking behavior of FRC. As well known, concrete is an inhomogeneous and brittle material. Its stress-strain curve is nonlinear and appears somewhat ductile. However, with a proper dosage of fibers, the degree of ductility in FRC concrete can be opportunely improved [Concrete Society 2003]. After initial diffusion of radial cracks from the loaded area to the outer elastic region, the post cracking capacity of the FRC slabs allows for a redistribution of moments, which let the FRC slab behave in a ductile manner, thus remarkably increasing its carrying capacity with respect to plain concrete. Failure of the plate is then due to the onset of a circumferential crack on the top of the slab.

The governing ODEs for adjacent regions of the plate are derived and solved in closed form in Section 2. Accordingly, the boundary conditions between adjacent regions at the onset of the circumferential crack are set in Section 3. Two admissible configurations are envisaged, depending on whether the circumferential crack occurs within the inner radially cracked region or the outer elastic region. Some details on the calculation of ultimate bending moments in FRC slab are recalled in Section 4, according to the recommendations of the Concrete Society [2003]. Analytical results are presented in Section 5 for different material and geometrical parameters. By matching the analytical results, a simplified equation is also proposed for the calculation of the load-bearing capacity of FRC slab on grade and compared with already known solutions. The obtained analytical results thus improve the findings of the rigid-plastic analyses based on the upper-bound theorem of limit analysis and agree with widely adopted relations derived from loading tests.

2. Governing equations

In the following, the load carrying capacity of an infinite FRP-concrete plate resting on a Winkler-type elastic foundation is investigated by assuming elastic-perfectly plastic behavior of the plate obeying Johansen's yield criterion and associative flow rule. Moreover, bilateral contact is considered between plate and subgrade, so that the plate cannot lift off the subgrade.

Reference is made to a polar coordinate system (r, θ) whose origin lays at the center of the loaded area of radius a (Figure 1). The external load P is applied on the upper plate surface as a uniform pressure p over a small circle of radius a centered at the origin of the polar coordinates system (Figure 1), so that the distributed load intensity is $p = P/\pi a^2$. In order to avoid punching failure, the radius a should not be less than the thickness of the slab [Meyerhof 1960].

Both in the elastic and elastic-plastic regions of the plate, the equilibrium equations under axisymmetrical conditions require

$$(rm_r)' - m_\theta + rt_r = 0, \quad (1)$$

$$(rt_r)' + r(kw - p) = 0, \quad (2)$$

where the apex denotes derivative with respect to r , m_r and m_θ are the bending moments per unit length, t_r is the transverse shear force per unit length, whose positive directions are shown in Figure 2, right, w is the out-of-plane displacement, positive if directed towards the subgrade, and k is the subgrade modulus.

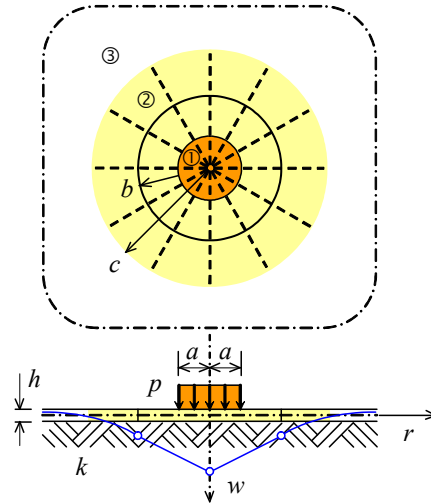


Figure 1. Loaded plate on elastic foundation, yield lines and plastic collapse mechanism: (1) elastic-plastic loaded region; (2) elastic-plastic unloaded region; (3) elastic region.

Under axisymmetrical conditions, all field variables depend on r only and, thus, they are independent of the angular coordinate θ .

Johansen’s square yield criterion is assumed to hold for the plate (Figure 2, left), namely

$$-m_0^- \leq m_r \leq m_0^+, \quad -m_0^- \leq m_\theta \leq m_0^+, \quad (3)$$

where m_0^+ and m_0^- are the positive and negative yield moments per unit length.

According to the Kirchhoff plate theory, the material fibers orthogonal to the midplane do not change their length but they just undergo a rigid rotation about the axes orthogonal to the radial direction, namely

$$\phi_\theta = -w'_3. \quad (4)$$

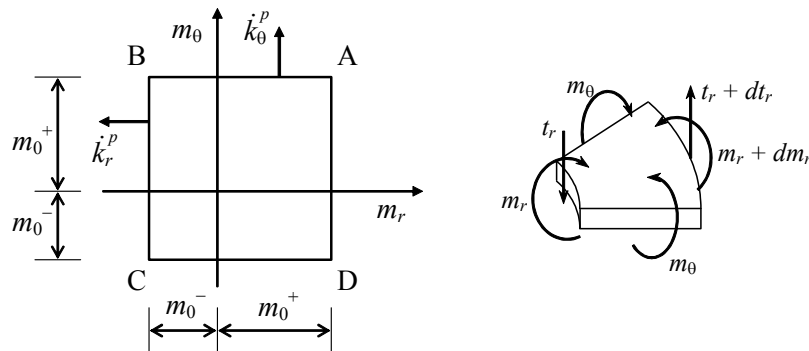


Figure 2. Left: Johansen’s yield locus for plates and flow rule for plastic curvatures k_θ^P and k_r^P . Right: positive bending moments and shear force for unit length.

If the plate is driven into the soil by increasing the load, at first positive plastic moments occur along radial yield lines up to a distance c to the center of the loaded area, where the yield condition

$$m_{\theta}(r) = m_0^+ \quad \text{for } r \leq c \quad (5)$$

is attained. Correspondingly, radial cracks form and propagate along the radial direction at the bottom of the slab. In line with Meyerhof [1962], the ultimate bearing capacity of the plate is attained as a circumferential crack takes place on the top of the slab at a distance b , which can be smaller, equal or larger than c , where the radial bending moment becomes equal to the negative yield moment, namely

$$m_r(b) = -m_0^-, \quad (6)$$

so that a circumferential crack originates on the top of the slab (Figure 1). Accordingly, the bending moment m_r attains a minimum at the radial distance $r = b$ to the center, namely:

$$m_r'(b) = 0. \quad (7)$$

Outside the circular region of radius c , the plate behaves elastically. Therefore, the distance c of the inner border of the elastic region is defined by the fulfillment of the yield condition (3), namely

$$m_{\theta}(c) = m_0^+. \quad (8)$$

Actually, the load-carrying capacity of the slab on grade is not exhausted after the formation of the circumferential crack, since the grade may carry further load. However, the usefulness and serviceability of the slab may be greatly impaired.

2.1. Elastic-perfectly plastic region. Let us consider the inner region of the plate for $r \leq c$, which undergoes elastic-perfectly plastic deformation and is subject to radial cracking at its bottom. Within this region, the bending moment m_{θ} attains its positive limit value m_0^+ according to the yield condition (5), which corresponds to the side AB of the yield locus (Figure 2, left). Under proportional loadings, the elastic-plastic constitutive equations for the bending moments are assumed in the integrated form

$$m_r = D(k_r^e + \nu k_{\theta}^e), \quad m_{\theta} = D(k_{\theta}^e + \nu k_r^e), \quad (9)$$

being $D = Eh^3/12(1 - \nu^2)$ the flexural rigidity of the plate, where h is the plate thickness, E is the Young modulus and ν is the Poisson coefficient of the material (approximately 0.15). The curvature tensor has been split into elastic and plastic contributions according to

$$k_r = k_r^e + k_r^p = -w''(r), \quad k_{\theta} = k_{\theta}^e + k_{\theta}^p = -w'(r)/r. \quad (10)$$

From (9) the following inverse constitutive relations can be derived for the elastic components of the curvature tensor

$$k_r^e = \frac{m_r - \nu m_{\theta}}{D(1 - \nu^2)}, \quad k_{\theta}^e = \frac{m_{\theta} - \nu m_r}{D(1 - \nu^2)}, \quad (11)$$

whereas the plastic components are given by the associative flow rule for the side AB of the yield locus, namely

$$k_r^p = 0, \quad k_{\theta}^p \geq 0, \quad (12)$$

where no previous plastic yielding is assumed to occur. Therefore, from (5), (10)–(12) and (1) the bending moment and the transverse shear force per unit length in the elastic-plastic region turn out to be

$$m_r = \nu m_0^+ - D(1 - \nu^2)w'', \quad (13)$$

$$t_r = \frac{1 - \nu}{r}[m_0^+ + D(1 + \nu)(w'' + rw''')], \quad (14)$$

respectively. From equilibrium Equations (1) and (2) and yield condition (5) it follows that

$$(rm_r)'' - r(kw - p) = 0. \quad (15)$$

Introduction of (13) into (15) then provides

$$D(1 - \nu^2)(rw'')'' + r(kw - p) = 0, \quad (16)$$

namely

$$w'''' + \frac{2}{r}w''' + \frac{1}{\ell^4(1 - \nu^2)}\left(w - \frac{p}{k}\right) = 0, \quad (17)$$

where

$$l = \sqrt[4]{\frac{D}{k}}, \quad (18)$$

is the characteristic length of plates on elastic foundation. The general solution of the fourth-order linear ODE (17) may be found by using the singular Frobenius method, implemented in Mathematica, in terms of the generalized hypergeometric function ${}_0F_3$ and Meijer G function G_{04}^{20} defined in the Appendix, namely

$$w_1(r) = \frac{p}{k} + \frac{m_0^+ \ell^2}{D} \left\{ b_0 {}_0F_3\left(\frac{1}{2}, \frac{3}{4}, \frac{3}{4}; -\frac{(1 - \nu^2)r^4}{256\ell^4}\right) + b_1 \frac{r}{4\ell} {}_0F_3\left(\frac{3}{4}, 1, \frac{5}{4}; -\frac{(1 - \nu^2)r^4}{256\ell^4}\right) \right. \\ \left. + b_2 \left(\frac{r}{4\ell}\right)^2 {}_0F_3\left(\frac{5}{4}, \frac{5}{4}, \frac{3}{2}; -\frac{(1 - \nu^2)r^4}{256\ell^4}\right) + b_3 G_{04}^{20}\left(\begin{matrix} 0 & 0 & 0 & 0 \\ 1/4 & 1/4 & 1/2 & 0 \end{matrix} \middle| -\frac{(1 - \nu^2)r^4}{256\ell^4}\right) \right\}. \quad (19)$$

The displacement field (19) holds for $r \leq a$, namely within the inner circular region loaded by p , whereas the displacement field

$$w_2(r) = \frac{m_0^+ \ell^2}{D} \left\{ c_0 {}_0F_3\left(\frac{1}{2}, \frac{3}{4}, \frac{3}{4}; -\frac{(1 - \nu^2)r^4}{256\ell^4}\right) + c_1 \frac{r}{4\ell} {}_0F_3\left(\frac{3}{4}, 1, \frac{5}{4}; -\frac{(1 - \nu^2)r^4}{256\ell^4}\right) \right. \\ \left. + c_2 \left(\frac{r}{4\ell}\right)^2 {}_0F_3\left(\frac{5}{4}, \frac{5}{4}, \frac{3}{2}; -\frac{(1 - \nu^2)r^4}{256\ell^4}\right) + c_3 G_{04}^{20}\left(\begin{matrix} 0 & 0 & 0 & 0 \\ 1/4 & 1/4 & 1/2 & 0 \end{matrix} \middle| -\frac{(1 - \nu^2)r^4}{256\ell^4}\right) \right\}, \quad (20)$$

holds for $a \leq r \leq c$, namely within the elastic-plastic annular region subject to the subgrade reaction only ($p = 0$). The general solutions (19) and (20) of the ODE (17) agree with the results obtained by Sokól-Supel [1985; 1988] and Kocatürk [1997] in terms of infinite power series. The derivatives up to the third order of the functions $w_1(r)$ and $w_2(r)$ are supplied in the Appendix.

2.2. Elastic region. Under axisymmetric bending, the Kirchhoff theory of elastic plates resting on a Winkler-type elastic foundation [Timoshenko and Woinowsky-Krieger 1959] provides the following ODE for the out-of-plane displacement $w(r)$

$$w'''' + \frac{2}{r}w''' - \frac{1}{r^2}w'' + \frac{1}{r^3}w' + \frac{1}{\ell^4}w = 0. \tag{21}$$

The general solution of the ODE (21) vanishing as r becomes very large are given by Timoshenko and Woinowsky-Krieger [1959] in the form

$$w_3(r) = \frac{m_0^+ \ell^2}{D} \left(d_1 \operatorname{ker} \frac{r}{\ell} + d_2 \operatorname{kei} \frac{r}{\ell} \right), \quad \text{for } r \geq c, \tag{22}$$

where ker and kei are the Kelvin functions [Abramowitz and Stegun 1964] and d_1 and d_2 are nondimensional arbitrary constants of integration. The derivatives up to the third order of the function $w_3(r)$ are supplied in the Appendix.

In agreement with the constitutive relations (9), bending moments per unit length for purely elastic response of the plate can be written in terms of the total curvatures as

$$m_r = -D \left(w_3'' + \frac{\nu}{r} w_3' \right), \tag{23}$$

$$m_\theta = -D \left(\frac{w_3'}{r} + \nu w_3'' \right), \tag{24}$$

whereas the transverse shear force per unit length can be obtained from the introduction of the bending moments (23) and (24) into the equilibrium condition (1) as

$$t_r = D \left(w_3''' + \frac{1}{r} w_3'' - \frac{1}{r^2} w_3' \right). \tag{25}$$

3. Boundary conditions

The nondimensional constants of integration b_k, c_k ($k = 0, 1, 2, 3$), d_1 and d_2 introduced in (19), (20) and (22) can be determined by imposing the boundary conditions at $r = 0$ and $r \rightarrow \infty$ and continuity conditions for the displacement w , rotation ϕ_θ , bending moment m_r and shear force t_r between the three different regions delimited by the radii a and c , together with the yield condition (8) at the inner border of the elastic region.

The yield condition (5) and symmetry at $r = 0$ require $m_r(0) = m_0^+$ and $t_r(0) = 0$. By using (13), (14) and (19) both of these conditions provide

$$D(1 + \nu)w_1''(0) + m_0^+ = 0, \tag{26}$$

thus implying

$$b_2 = -\frac{8}{1 + \nu}. \tag{27}$$

Moreover, boundedness of the rotation ϕ_θ at $r = 0$ necessarily requires

$$b_3 = 0. \tag{28}$$

Continuity of displacement w , rotation ϕ_θ , bending moment m_r and shear force t_r across the boundaries at $r = a$ and $r = c$, by using (4), (13), (14), (23) and (25) then requires the eight conditions

$$w_1(a) = w_2(a), \quad w'_1(a) = w'_2(a), \quad w''_1(a) = w''_2(a), \quad w'''_1(a) = w'''_2(a), \quad (29)$$

$$w_2(c) = w_3(c), \quad w'_2(c) = w'_3(c), \quad (30)$$

$$\frac{\nu m_0^+}{D} - (1 - \nu^2)w''_2(c) = -w'''_3(c) - \frac{\nu}{c}w'_3(c), \quad (31)$$

$$(1 - \nu)\frac{m_0^+}{D} + (1 - \nu^2)[w''_2(c) + cw'''_2(c)] = cw'''_3(c) + w'''_3(c) - \frac{1}{c}w'_3(c). \quad (32)$$

By using (24), fulfillment of the yield condition (8) as r approaches c from above then implies

$$\nu w'''_3(c) + \frac{1}{c}w'_3(c) = -\frac{m_0^+}{D}. \quad (33)$$

The ultimate distributed load $p = p_0$ is attained as soon as the bending moment m_r obeys the yield condition (6) at a distance b determined by the minimum condition (7). Let us first assume that the circumferential crack occurs within the elastic plastic unloaded region, namely for $a < b < c$. Then, by using (13), conditions (6) and (7) become

$$D(1 - \nu^2)w''_2(b) = (\nu + \mu)m_0^+, \quad w'''_2(b) = 0, \quad (34)$$

with $b \leq c$, where

$$\mu = m_0^- / m_0^+, \quad (35)$$

is the ratio between negative and positive yield moments. If conditions (34) provide $b > c$ then the minimum value of the radial bending moment $m_r = -m_0^-$ is attained within the elastic region at $r = b$, where a circumferential crack occurs on the top of the slab. In this case, by using (23) conditions (6) and (7) require

$$w'''_3(b) + \frac{\nu}{b}w'_3(b) = \mu \frac{m_0^+}{D}, \quad w'''_3(b) + \frac{\nu}{b}w'''_3(b) - \frac{\nu}{b^2}w'_3(b) = 0, \quad (36)$$

with $c < b$, instead of (34).

By introducing the derivatives of function w_k ($k = 1, 2, 3$) provided in the Appendix, the boundary conditions (29)–(33) yield a linear system of nine equations for the eight constants of integration $b_0, b_1, c_0, c_1, c_2, c_3, d_1, d_2$ and the ultimate distributed load p_0 , which can be solved by using Mathematica. Once these nine constants are known in terms of the parameters b and c , the two Equations (34) can be solved numerically (using the command FindRoot in Mathematica) in order to obtain the last two unknowns b and c . If conditions (34) provide $b > c$ then conditions (36) must replace the former. Once the values of b and c have been obtained, all the unknown constants can be consequently calculated. In particular, the ultimate load is then given by

$$P_0 = \pi a^2 p_0. \quad (37)$$

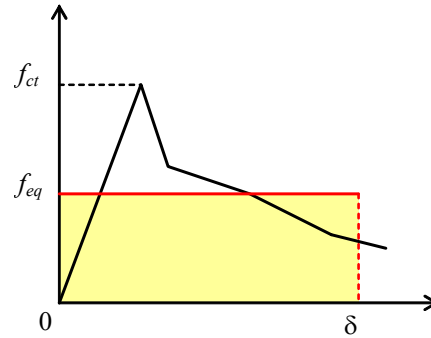


Figure 3. Equivalent flexural strength (vertical axis) versus deflection determined from a third-point loading beam.

4. Moment-carrying capacity for FRC slabs

As remarked, for design purposes it is assumed that the limiting criterion is the onset of cracking on the top surface. While fibers increase the post-cracking behavior and thus the ductility of the slab they do not affect the cracking stress, namely they do not increase the negative bending moment capacity [Soutsos et al. 2012] which is therefore the same of the plain concrete

$$m_0^- = m_0^{\text{PC}} = f_{ct} \frac{h^2}{6}, \quad (38)$$

where f_{ct} the maximum tensile stress derived from a third-point flexural test on a FRC beam.

According to the design method for industrial floor proposed by the Concrete Society [2003], the difference between plain concrete and FRC slabs can be attributed to the post-cracking strength due to the presence of the fibers, which provide an additional contribution to the bending moment capacity, namely

$$m_0^{\text{FRC}} = \frac{R_{e,3}}{100} f_{ct} \frac{h^2}{6}, \quad (39)$$

where $R_{e,3}$ is the residual flexural strength ratio

$$R_{e,3} = \frac{f_{eq}}{f_{ct}} 100, \quad (40)$$

and f_{eq} is the equivalent flexural strength for a deflection of 1/150 of the test beam span (Figure 3), namely $\delta = 3$ mm for a span of 450 mm. The ratio $R_{e,3}$ is related to the rate of improvement in the flexural strength of FRC compared to plain concrete, according to standard third-point flexural test [Concrete Society 2003].

The ductility of FRC slabs becomes effective after the first crack, namely in the plastic phase when a positive plastic hinge is formed under loading. In this case due to the post-cracking behavior of the fibers, the FRC slab can bear a further increase in the value of the positive bending moment with respect to the plain concrete, so that the total value of the moment-carrying capacity is given by the sum

$$m_0^+ = m_0^{\text{PC}} + m_0^{\text{FRC}} = \left(1 + \frac{R_{e,3}}{100}\right) f_{ct} \frac{h^2}{6}, \quad (41)$$

where m_0^+ is the ultimate positive bending moment. Therefore, for FRC slabs the ratio μ between negative and positive yield moments introduced in (35) turns out to be

$$\mu = \frac{100}{100 + R_{e,3}}. \quad (42)$$

5. Results

The nondimensional variations of displacement w and bending moments m_r and m_θ along the radial direction under the ultimate load p_0 are plotted in Figure 4 for different sizes a of the loaded area, for $\nu = 0.15$ and for two different values of the ratio μ between negative and positive yield moments, namely $\mu = 0.5$ and $\mu = 1$. Figure 4 shows that the displacement w and thus the reaction kw of the subgrade increase with the size a of the loaded area. Figure 4 also shows that all quantities of interest (deflection, tangential and radial moments) become negligible at a distance larger than 4 to 5 times ℓ (denoted by $4-5\ell$) from the applied load. Therefore, the assumption of an infinitely large plate is reliable also for plates of finite size, if they are loaded at a distance larger than $4-5\ell$ from their edges.

The nondimensional variations of the ultimate load P_0 and radii b and c with the radius a of the loaded area are plotted in Figures 5 and 6, respectively, both for $\mu = 1$ and $\mu = 0.5$. From these figures it can be observed that the ultimate load P_0 increases with the radius a of the loaded area. Moreover, the radius b of the circumferential crack turns out to be smaller than 2ℓ . It must be remarked that the minimum of the radial bending moment predicted by the elastic analyses of Meyerhof [1960] and Timoshenko and Woinowsky-Krieger [1959] is attained at a distance 2ℓ to the center of the loaded area, and this value has been adopted as the radius of the circumferential crack in several investigations based on the limit analysis theory [Westergaard 1948; Baumann and Weisgerber 1983].

As the size a of the loaded area becomes larger, the radius b of the circumferential crack increases more rapidly than the length c of the radial cracks (Figure 6) and the latter two distances become coincident for a special value of a . Then, the circumferential crack occurs within the elastic region for a larger than this special value. In this case, however, the onset of the circumferential crack does not imply the activation of a conical plastic mechanism as observed for a small value of a . However, the formation of a circumferential crack on upper side of the plate defines the serviceability limit of industrial ground floors according to current design standards [Concrete Society 2003].

For use in practice, the following simplified equation for calculating the load-carrying capacity of slabs on grade is proposed on the basis of the analytical results here obtained:

$$P_0^* = 2\pi m_0^+ (1 + \mu) \left(1 + (1 + \mu) \frac{a}{\ell} \right), \quad (43)$$

where μ assumes the value in (42) for FRC slabs. From Figure 5 it can be established that the approximate value P_0^* introduced in (43) approaches the load carrying capacity P_0 obtained from the present exact analysis. From Table 1, where the values of P_0 and P_0^* are reported for different sizes of the loaded area, it can be observed that the agreement between analytical and approximate results is excellent for $\mu = 1$, whereas for $\mu = 0.5$ the approximate value P_0^* underestimates to some extent the ultimate load P_0 , thus providing more conservative results.

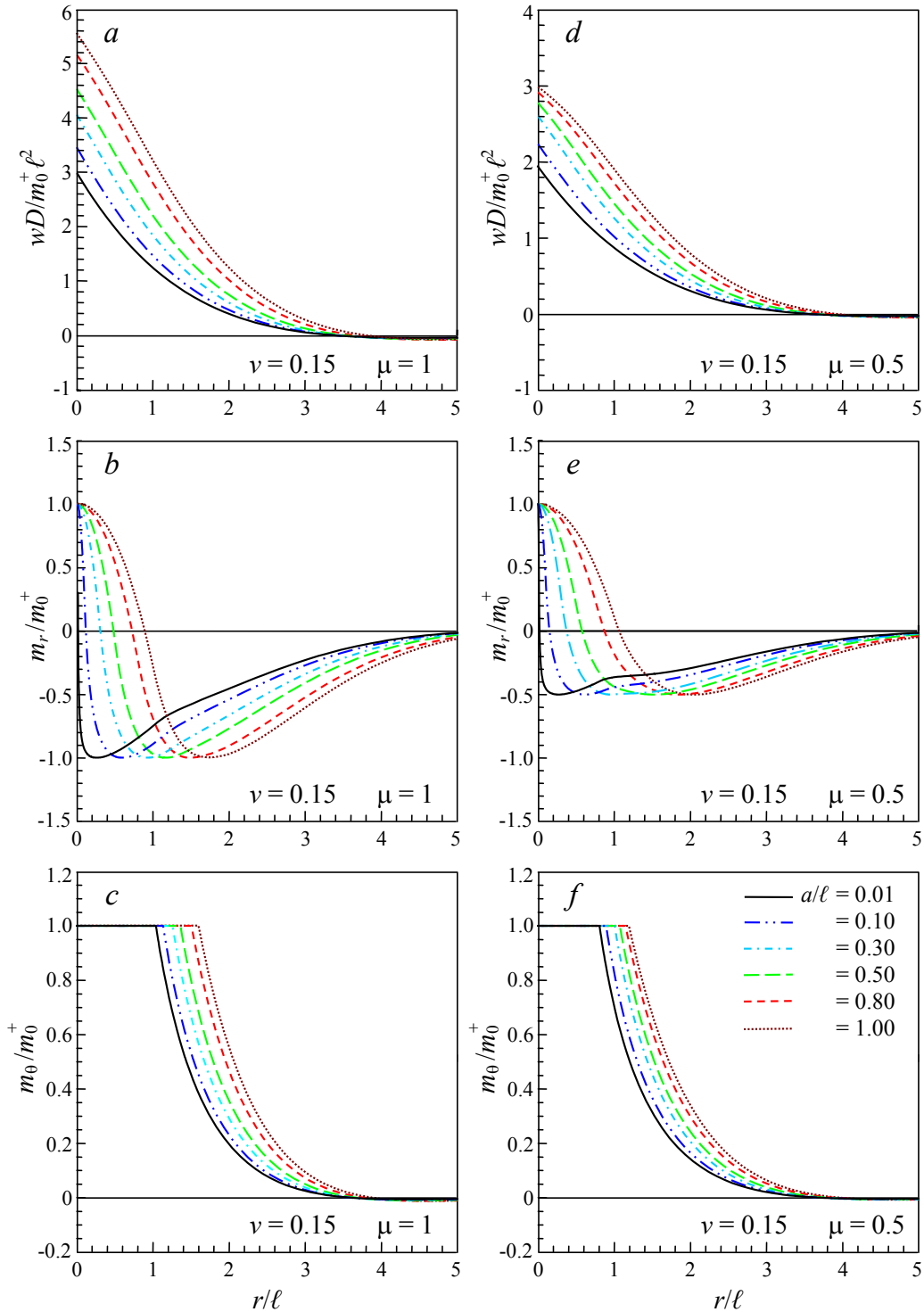


Figure 4. Variations of displacement w and bending moments m_r and m_θ along the radial direction under the collapse load for different sizes a of the loaded area.

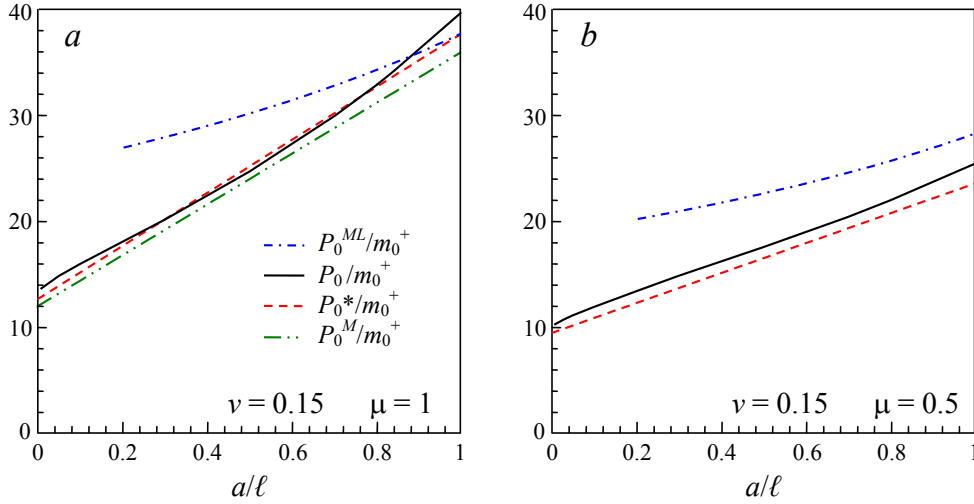


Figure 5. Nondimensional variations of the ultimate load P_0 , approximate value P_0^* and Meyerhof collapse loads P_0^{ML} and P_0^M with the radius a of the loaded area for (a) $\mu = 1$ and (b) $\mu = 0.5$.

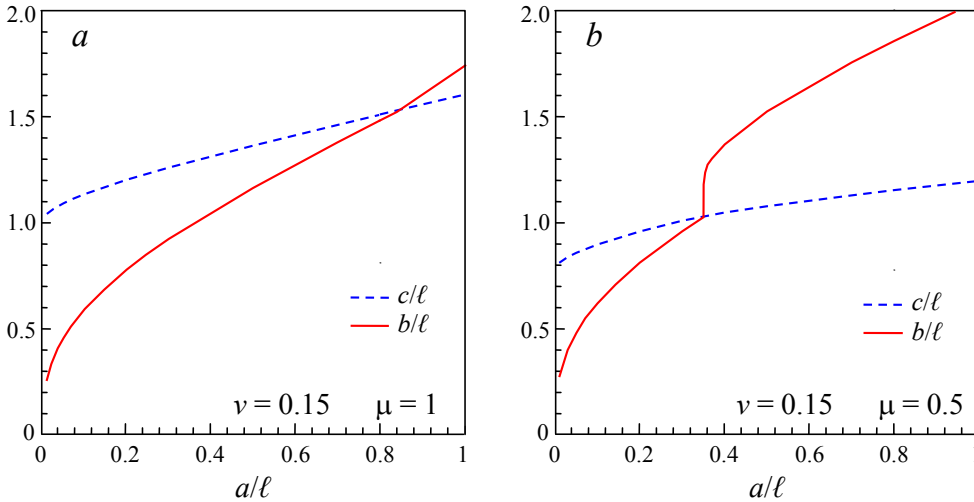


Figure 6. Nondimensional variations of the radii b and c with the radius a of the loaded area.

5.1. Comparison with previous methods. In the following, the load-carrying capacities found in previous investigations are reported in order to compare them with the predictions of the present analysis. For a large slab Meyerhof [1962] found the ultimate load

$$P_0^{ML} = \frac{4\pi(m_0^+ + m_0^-)}{1 - \frac{a}{3\ell}}, \quad \text{for } a > 0.2\ell, \tag{44}$$

where the assumption $b \approx 3.9-4\ell$ is made. It must be specified that in the rigid-plastic analysis of

$\mu = 1$			$\mu = 0.5$		
a/ℓ	P_0/m_0^+	P_0^*/m_0^+	a/ℓ	P_0/m_0^+	P_0^*/m_0^+
0.01	13.6942	12.8177	0.01	10.2513	9.4247
0.05	14.8298	13.8230	0.05	11.0604	10.1316
0.10	15.9689	15.0796	0.10	11.8682	10.8385
0.20	18.0721	17.5929	0.20	13.3502	12.2522
0.30	20.1759	20.1062	0.30	14.8202	13.6659
0.40	22.3747	22.6195	0.40	16.2143	15.0796
0.50	24.7162	25.1327	0.50	17.5310	16.4934
0.70	29.9581	30.1593	0.70	20.3785	19.3208
0.80	32.9149	32.6726	0.80	21.9421	20.7345
1.00	39.5404	37.6991	1.00	25.4027	23.5619

Table 1. Ultimate load P_0 and its approximate value P_0^* for different radii a of the loaded area, for $\mu = 1$ (left) and $\mu = 0.5$ (right).

[Meyerhof 1962], the cracking radius b is assumed to coincide with the radius of the circular area loaded by the subgrade reaction pressure. In the present elastic-perfectly plastic analysis the circumferential crack is found to occur much inside the area loaded by the subgrade reaction pressure. The results depicted in Figure 6 show that the assumption $b \approx 3.9-4\ell$ [Meyerhof 1962] made in the derivation of (44) may be acceptable for the size of the area loaded by the subgrade reaction pressure (see Figures 5(a) and 5(d)), but is rather inaccurate for the cracking radius. The present analysis, indeed, predicts a cracking radius b about $1-1.5\ell$ (see Figure 6) and thus much smaller than the value assumed in the derivation of (44). The load-carrying capacity (44) predicted by Meyerhof [1962] would remarkably increases if values of b smaller than 4ℓ are considered, e.g., $b \leq 2\ell$, thus providing non conservative and unrealistic results.

The load-carrying capacity of the plate under a concentrated load provided by Meyerhof [1962] is

$$P_0^{ML} = 2\pi(m_0^+ + m_0^-) \quad \text{for } a = 0. \tag{45}$$

It can be observed that for a vanishing small size a of the loaded area, Equation (43) coincides with the result (45) obtained by Meyerhof under a concentrated force.

The use of $m_0^- = 0$ in Equations (44) and (45) is recommended for small slabs that can not develop a negative bending moment along the negative circumferential yield line [Meyerhof 1962]. In this case, the load-carrying capacity of small slabs P_0^{MS} is reduced to about one-half with respect to a large slab, and thus expressions (44) and (45) may be too conservative if adopted for sufficiently large slabs with $m_0^- = 0$. However, similar expressions have also been accepted by the Concrete Society [2003], with no specification about the extension of the slab.

On the basis of the results of both limit analysis theory and loading tests, the following simple and conservative formula is suggested in [Meyerhof 1962] for a central load

$$P_0^M = 6(m_0^+ + m_0^-) \left(1 + 2\frac{a}{\ell}\right), \tag{46}$$

with $a > h$ in order to avoid punching failure. Moreover, the following approximate relation for the radius of the circumferential crack

$$\frac{b}{\ell} = 1.63 \sqrt{\frac{a}{\ell}}, \quad (47)$$

was also proposed by Meyerhof [1960]. Relations (46) and (47) reasonably agree with the analytical results here obtained for elastic-perfectly plastic behavior of the plate, with $\mu = 1$, as it can be verified by comparing Equations (46) and (43) and the results plotted in Figures 5(a) and 7(b). In particular, the difference between relations (46) and (43) is less than 5%, for $\mu = 1$. On the contrary, the load carrying capacity (44) predicted by Meyerhof for large slabs turns out to be much higher than the findings of the present analysis. As already discussed, this result is expected according to the upper-bound theorem of limit analysis, since the Meyerhof analysis is based on the assumption of a rigid-plastic mechanism.

The ultimate load proposed by Baumann and Weisgerber [1983] is

$$P_0^{\text{BW}} = \frac{8\pi(m_0^+ + m_0^-)}{3(1 - \frac{a}{3\ell})^2} \left(1 - \frac{11a}{32\ell}\right), \quad (48)$$

where the same cracking radius $b = 2\ell$ predicted by the elastic solution [Westergaard 1948; Timoshenko and Woinowsky-Krieger 1959] has been considered.

The ultimate load found by Rao and Singh [1986] for a single plastic hinge centered under the loaded area becomes

$$P_0^{\text{RS}} = 2\pi(m_0^+ + m_0^-) \frac{1.8 + 6.9a/\ell}{1.8 + 2.9a/\ell}. \quad (49)$$

These authors evaluated the cracking radius b throughout the following relation

$$\frac{b}{\ell} = 0.6 + 2.3 \frac{a}{\ell}, \quad (50)$$

derived from a hundred experimental observations made for plain and reinforced concrete.

The load-carrying capacities P_0 and the cracking radius b predicted by the present model and by previously developed analyses are compared for $\mu = 1$ in Figures 7(a) and 7(b), respectively. From these plots it can be observed that the present model provides higher load-carrying capacities than the other models, except for the result (44) obtained by Meyerhof [1962] for large slabs. Moreover, the radius b of the circumferential crack predicted by the present analysis closely agrees with the approximation (47) proposed by Meyerhof [1960], at least for $\mu = 1$, whereas it is clearly smaller than the value 2ℓ predicted by the elastic analyses and that adopted by Rao and Singh [1986] for the derivation of (50).

Unfortunately, experimental results are not easily available in the literature for slabs larger than 8–10 ℓ , thus allowing the formation of a circumferential crack. Most of the performed tests concern small slabs whose collapse mechanism consists of radial cracks reaching the edges of the slab, with no formation of the circumferential crack on the top surface [Chen 2004; Roesler et al. 2004; 2006].

6. Conclusions

A refined model for the evaluation of the load-carrying capacity of large FRC slabs on ground has been presented here. The model takes into account the post-crack strength of FRC slabs and the associated ductile behavior. Compared with the approaches based on the limit analysis theory, the present model is

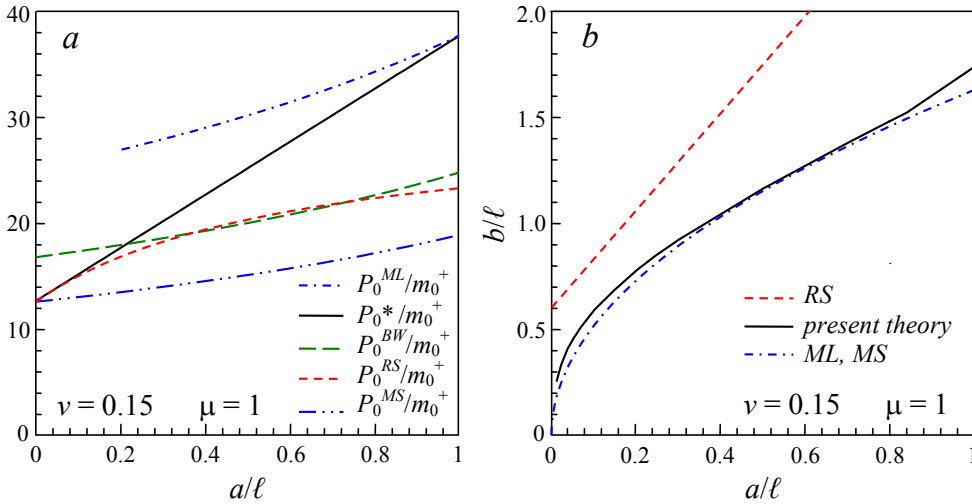


Figure 7. Comparison between the load-carrying capacity P_0 and cracking radius b predicted by the present model and by previous theories.

more accurate and complete, since it does not require the introduction of rough approximations on the collapse mechanism and location of the yield lines. The proposed approach provides more conservative results with respect to the prediction of the Meyerhof model for large slabs. However, it is in reasonable agreement with the approximate formula (46) suggested by Meyerhof [1962] on the basis of loading tests. Moreover, the load-carrying capacity provided by the present method turns out to be higher than those recommended by conventional codes for industrial ground floors [Concrete Society 2003], which are generally based on the results of Meyerhof analysis for small slabs on grade.

Differently from the investigations based on limit analysis, the present model is also able to predict the deflection under the ultimate load, and thus it can be validated by comparison with experimental results. Moreover, being deflection a crucial aspect for the design of ground slab, deflection limiting criteria can be easily implemented within the framework of the present method.

The interaction between slab and subgrade has been here modeled by adopting the simple Winkler elastic model. However, more refined approaches can be envisaged within the same framework, which can take into account for tensionless subgrade reaction [Gazetas 1981; Silva et al. 2001], frictional contact [Chen 2004] and nonlocal response of the foundation, like the model adopted by Nobili et al. [2014] and Lanzoni et al. [2014] for the study of cracked elastic plates on Pasternak foundation.

Finally, it must be remarked that a large moment-rotation capacity after yielding must be assured, the present approach being based on the yield line method, commonly used to determine the load capacity of ductile and RC slabs. However, application of the present results to materials exhibiting brittle or softening behavior, like lightly reinforced concrete, may be questionable.

Appendix

By using the following derivative rule for the hypergeometric function ${}_0F_3$ and Meijer G function G_{04}^{20}

[Luke 1969; Lardner 1969]

$$\begin{aligned} \frac{d}{dx} {}_0F_3(\alpha, \beta, \gamma; x) &= \frac{1}{\alpha\beta\gamma} {}_0F_3(\alpha + 1, \beta + 1, \gamma + 1; x), \\ \frac{d}{dx} G_{04}^{20} \left(\begin{matrix} 0 & 0 & 0 & 0 \\ \alpha & \alpha & \beta & 0 \end{matrix} \middle| x \right) &= G_{04}^{20} \left(\begin{matrix} 0 & 0 & 0 & 0 \\ \alpha - 1 & \alpha - 1 & \beta - 1 & 0 \end{matrix} \middle| x \right), \end{aligned} \quad (\text{A.1})$$

the derivatives up to the third order with respect to r of the function $w_1(r)$ introduced in (19) can be written as

$$\begin{aligned} w_1'(r) &= \frac{m_0^+ \ell}{D} \left\{ -b_0 \frac{(1-v^2)r^3}{18\ell^3} {}_0F_3 \left(\frac{3}{2}, \frac{7}{4}, \frac{7}{4}; -\frac{(1-v^2)r^4}{256\ell^4} \right) \right. \\ &\quad + b_1 \left[\frac{1}{4} {}_0F_3 \left(\frac{3}{4}, 1, \frac{5}{4}; -\frac{(1-v^2)r^4}{256\ell^4} \right) - \frac{(1-v^2)r^4}{240\ell^4} {}_0F_3 \left(\frac{7}{4}, 2, \frac{9}{4}; -\frac{(1-v^2)r^4}{256\ell^4} \right) \right] \\ &\quad + b_2 \left[\frac{r}{8\ell} {}_0F_3 \left(\frac{5}{4}, \frac{5}{4}, \frac{3}{2}; -\frac{(1-v^2)r^4}{256\ell^4} \right) - \frac{(1-v^2)r^5}{2400\ell^5} {}_0F_3 \left(\frac{9}{4}, \frac{9}{4}, \frac{5}{2}; -\frac{(1-v^2)r^4}{256\ell^4} \right) \right] \\ &\quad \left. - b_3 \frac{(1-v^2)r^3}{64\ell^3} G_{04}^{20} \left(\begin{matrix} 0 & 0 & 0 & 0 \\ -3/4 & -3/4 & -1/2 & 0 \end{matrix} \middle| -\frac{(1-v^2)r^4}{256\ell^4} \right) \right\}, \end{aligned} \quad (\text{A.2})$$

$$\begin{aligned} w_1''(r) &= \frac{m_0^+}{D} \left\{ b_0 \frac{(1-v^2)r^2}{6\ell^2} \left[\frac{(1-v^2)r^4}{882\ell^4} {}_0F_3 \left(\frac{5}{2}, \frac{11}{4}, \frac{11}{4}; -\frac{(1-v^2)r^4}{256\ell^4} \right) - {}_0F_3 \left(\frac{3}{2}, \frac{7}{4}, \frac{7}{4}; -\frac{(1-v^2)r^4}{256\ell^4} \right) \right] \right. \\ &\quad + b_1 \frac{(1-v^2)r^3}{48\ell^3} \left[\frac{(1-v^2)r^4}{2520\ell^4} {}_0F_3 \left(\frac{11}{4}, 3, \frac{13}{4}; -\frac{(1-v^2)r^4}{256\ell^4} \right) - {}_0F_3 \left(\frac{7}{2}, 2, \frac{9}{4}; -\frac{(1-v^2)r^4}{256\ell^4} \right) \right] \\ &\quad + \frac{b_2}{2400} \left[300 {}_0F_3 \left(\frac{5}{4}, \frac{5}{4}, \frac{3}{2}; -\frac{(1-v^2)r^4}{256\ell^4} \right) - 7 \frac{(1-v^2)r^4}{\ell^4} {}_0F_3 \left(\frac{9}{4}, \frac{9}{4}, \frac{5}{2}; -\frac{(1-v^2)r^4}{256\ell^4} \right) \right. \\ &\quad \left. + \frac{(1-v^2)^2 r^8}{810\ell^8} {}_0F_3 \left(\frac{13}{4}, \frac{13}{4}, \frac{7}{2}; -\frac{(1-v^2)r^4}{256\ell^4} \right) \right] \\ &\quad - b_3 \frac{(1-v^2)r^2}{64\ell^2} \left[3 G_{04}^{20} \left(\begin{matrix} 0 & 0 & 0 & 0 \\ -3/4 & -3/4 & -1/2 & 0 \end{matrix} \middle| -\frac{(1-v^2)r^4}{256\ell^4} \right) \right. \\ &\quad \left. - \frac{(1-v^2)r^4}{64\ell^4} G_{04}^{20} \left(\begin{matrix} 0 & 0 & 0 & 0 \\ -7/4 & -7/4 & -3/2 & 0 \end{matrix} \middle| -\frac{(1-v^2)r^4}{256\ell^4} \right) \right] \right\}, \end{aligned} \quad (\text{A.3})$$

$$\begin{aligned} w_1'''(r) &= \frac{m_0^+}{D\ell} \left\{ b_0 \frac{(1-v^2)r}{3\ell} \left[-\frac{(1-v^2)^2 r^8}{2134440\ell^8} {}_0F_3 \left(\frac{7}{2}, \frac{15}{4}, \frac{15}{4}; -\frac{(1-v^2)r^4}{256\ell^4} \right) \right. \right. \\ &\quad \left. + \frac{(1-v^2)r^4}{196\ell^4} {}_0F_3 \left(\frac{5}{2}, \frac{11}{4}, \frac{11}{4}; -\frac{(1-v^2)r^4}{256\ell^4} \right) - {}_0F_3 \left(\frac{3}{2}, \frac{7}{4}, \frac{7}{4}; -\frac{(1-v^2)r^4}{256\ell^4} \right) \right] \\ &\quad + b_1 \frac{(1-v^2)r^2}{10080\ell^2} \left[-\frac{(1-v^2)^2 r^8}{20592\ell^8} {}_0F_3 \left(\frac{15}{4}, 4, \frac{17}{4}; -\frac{(1-v^2)r^4}{256\ell^4} \right) \right. \\ &\quad \left. + \frac{(1-v^2)r^4}{\ell^4} {}_0F_3 \left(\frac{11}{4}, 3, \frac{13}{4}; -\frac{(1-v^2)r^4}{256\ell^4} \right) - 630 {}_0F_3 \left(\frac{7}{4}, 2, \frac{9}{4}; -\frac{(1-v^2)r^4}{256\ell^4} \right) \right] \\ &\quad + b_2 \frac{(1-v^2)r^3}{129600\ell^3} \left[-\frac{(1-v^2)^2 r^8}{35490\ell^8} {}_0F_3 \left(\frac{17}{4}, \frac{17}{4}, \frac{9}{2}; -\frac{(1-v^2)r^4}{256\ell^4} \right) \right. \\ &\quad \left. + \frac{(1-v^2)r^4}{\ell^4} {}_0F_3 \left(\frac{13}{4}, \frac{13}{4}, \frac{7}{2}; -\frac{(1-v^2)r^4}{256\ell^4} \right) - 1620 {}_0F_3 \left(\frac{9}{4}, \frac{9}{4}, \frac{5}{2}; -\frac{(1-v^2)r^4}{256\ell^4} \right) \right] \end{aligned}$$

$$\begin{aligned}
 & -b_3 \frac{(1-\nu^2)r}{4096\ell} \left[384G_{04}^{20} \left(\begin{array}{cccc|c} 0 & 0 & 0 & 0 & -\frac{(1-\nu^2)r^4}{256\ell^4} \\ -3/4 & -3/4 & -1/2 & 0 & \end{array} \right) \right. \\
 & + 9 \frac{(1-\nu^2)r^4}{\ell^4} G_{04}^{20} \left(\begin{array}{cccc|c} 0 & 0 & 0 & 0 & -\frac{(1-\nu^2)r^4}{256\ell^4} \\ -7/4 & -7/4 & -3/2 & 0 & \end{array} \right) \\
 & \left. - \frac{(1-\nu^2)^2r^8}{64\ell^8} G_{04}^{20} \left(\begin{array}{cccc|c} 0 & 0 & 0 & 0 & -\frac{(1-\nu^2)r^4}{256\ell^4} \\ -11/4 & -11/4 & -5/2 & 0 & \end{array} \right) \right] \Bigg\}, \tag{A.4}
 \end{aligned}$$

respectively. Similar expressions hold for the derivatives of $w_2(r)$, but the constants b_k are replaced by c_k ($k = 0, 1, 2, 3$). The derivatives of $w_3(r)$ with respect to r up to the third order are

$$w'_3(r) = \frac{m_0^+ \ell}{\sqrt{2D}} [d_1 \Sigma(r) + d_2 \Delta(r)], \tag{A.5}$$

$$w''_3(r) = \frac{m_0^+}{\sqrt{2D}} \left\{ -d_1 \left[\sqrt{2} \operatorname{kei} \frac{r}{\ell} + \frac{\ell}{r} \Sigma(r) \right] + d_2 \left[\sqrt{2} \operatorname{ker} \frac{r}{\ell} - \frac{\ell}{r} \Delta(r) \right] \right\}, \tag{A.6}$$

$$w'''_3(r) = \frac{m_0^+}{\sqrt{2D}\ell} \left\{ d_1 \left[2 \frac{\ell^2}{r^2} \Sigma(r) + \sqrt{2} \frac{\ell}{r} \operatorname{kei} \frac{r}{\ell} - \Delta(r) \right] + d_2 \left[2 \frac{\ell^2}{r^2} \Delta(r) - \sqrt{2} \frac{\ell}{r} \operatorname{ker} \frac{r}{\ell} + \Sigma(r) \right] \right\}, \tag{A.7}$$

respectively, where

$$\Sigma(r) = \operatorname{ker} \frac{r}{\ell} + \operatorname{kei} \frac{r}{\ell}, \quad \Delta(r) = \operatorname{ker} \frac{r}{\ell} - \operatorname{kei} \frac{r}{\ell}. \tag{A.8}$$

Acknowledgements

Financial support from “Fondazione Cassa di Risparmio di Modena” within the framework of the International Research Project 2009–2010 “Modelling of crack propagation in complex materials” is gratefully acknowledged.

References

- [Abramowitz and Stegun 1964] M. Abramowitz and I. A. Stegun, *Handbook of mathematical functions with formulas, graphs, and mathematical tables*, National Bureau of Standards Applied Mathematics Series **55**, U.S. Government Printing Office, Washington, DC, 1964. Reprinted by Dover, New York, 1974.
- [Barros and Figueiras 1998] J. A. O. Barros and J. A. Figueiras, “Experimental behaviour of fibre concrete slabs on soil”, *Mech. Cohes. Frict. Mater.* **3**:3 (1998), 277–290.
- [Barros and Figueiras 1999] J. A. O. Barros and J. A. Figueiras, “Flexural behavior of SFRC: Testing and modeling”, *J. Mater. Civ. Eng. (ASCE)* **11**:4 (1999), 331–339.
- [Barros and Figueiras 2001] J. A. O. Barros and J. A. Figueiras, “Model for the analysis of steel fibre reinforced concrete slabs on grade”, *Comput. Struct.* **79** (2001), 97–106.
- [Baumann and Weisgerber 1983] R. Baumann and F. Weisgerber, “Yield-line analysis of slabs-on-grade”, *J. Struct. Eng. (ASCE)* **109**:7 (1983), 1553–1568.
- [Belenkiy 2007] L. Belenkiy, “Upper-bound solutions for rigid-plastic plates and slabs on elastic foundation by the principle of stationary total energy”, *J. Struct. Eng. (ASCE)* **133**:2 (2007), 305–307.
- [Bigoni and Piccolroaz 2004] D. Bigoni and A. Piccolroaz, “Yield criteria for quasibrittle and frictional materials”, *Int. J. Solids Struct.* **41**:11–12 (2004), 2855–2878.
- [Bischoff et al. 2003] P. Bischoff, A. Valsangkar, and J. Irving, “Use of fibers and welded-wire reinforcement in construction of slabs on ground”, *Pract. Period. Struct. Des. Constr.* **8**:1 (2003), 41–46.
- [Chen 2004] S. Chen, “Strength of steel fibre reinforced concrete ground slabs”, *Proc. Inst. Civ. Eng.* **157**:2 (2004), 157–163.

- [Concrete Society 2003] “Concrete industrial ground floors: A guide to design and construction”, Technical Report, Concrete Society, 2003, Available at <http://tinyurl.com/concrete-soc-TR34-2013>. Technical Report No. 34.
- [Falkner et al. 1995] H. Falkner, Z. Huang, and M. Teutsch, “Comparative study of plain and steel fiber reinforced concrete ground slabs”, *Concr. Int.* **17**:1 (1995), 45–51.
- [Gazetas 1981] G. C. Gazetas, “Ultimate behavior of continuous footings in tensionless contact with a three-parameter soil”, *J. Struct. Mech.* **9**:3 (1981), 339–362.
- [Gazetas and Tassios 1978] G. C. Gazetas and T. P. Tassios, “Elastic-plastic slabs on elastic foundation”, *J. Struct. Div. (ASCE)* **104**:4 (1978), 621–636.
- [Kocatürk 1997] T. Kocatürk, “Elastoplastic analysis of circular plates on elastoplastic foundation”, *J. Struct. Eng. (ASCE)* **123**:6 (1997), 808–815.
- [Lanzoni et al. 2014] L. Lanzoni, E. Radi, and A. Nobili, “Ultimate carrying capacity of elastic-plastic plates on Pasternak foundation”, *J. Appl. Mech. (ASME)* **81**:5 (2014), Article ID #051013.
- [Lardner 1969] T. J. Lardner, “Relations between ${}_0F_3$ and Bessel functions”, *SIAM Rev.* **11** (1969), 69–72.
- [Losberg 1978] A. Losberg, “Pavements and slabs on grade with structurally active reinforcement”, *ACI J.* **75**:11 (1978), 647–657.
- [Luke 1969] Y. L. Luke, *The special functions and their approximations, I and II*, Academic Press, New York, 1969.
- [Meyerhof 1960] G. G. Meyerhof, “Bearing capacity of floating ice sheets”, *J. Eng. Mech. Div. (ASCE)* **86**:EM3 (1960), 113–145.
- [Meyerhof 1962] G. G. Meyerhof, “Load-carrying capacity of concrete pavements”, *J. Soil Mech. Found. Div.* **88**:SM3 (1962), 89–116.
- [Nobili et al. 2014] A. Nobili, E. Radi, and L. Lanzoni, “A cracked infinite Kirchhoff plate supported by a two-parameter elastic foundation”, *J. Eur. Ceram. Soc.* **34**:11 (2014), 2737–2744.
- [Piccolroaz and Bigoni 2009] A. Piccolroaz and D. Bigoni, “Yield criteria for quasibrittle and frictional materials: A generalization to surfaces with corners”, *Int. J. Solids Struct.* **46**:20 (2009), 3587–3596.
- [Poltronieri et al. 2014] F. Poltronieri, A. Piccolroaz, D. Bigoni, and S. Romero-Baivier, “A simple and robust elastoplastic constitutive model for concrete”, *Eng. Struct.* **60** (2014), 81–84.
- [Rao and Singh 1986] K. S. S. Rao and S. Singh, “Concentrated load-carrying capacity of concrete slabs on ground”, *J. Struct. Eng. (ASCE)* **112**:12 (1986), 2628–2645.
- [Roesler et al. 2004] J. R. Roesler, D. A. Lange, S. A. Altoubat, K. A. Rieder, and G. R. Ulrich, “Fracture of plain and fiber-reinforced concrete slabs under monotonic loading”, *J. Mater. Civ. Eng. (ASCE)* **16**:5 (2004), 452–460.
- [Roesler et al. 2006] J. R. Roesler, S. A. Altoubat, D. A. Lange, K. A. Rieder, and G. R. Ulrich, “Effect of synthetic fibers on structural behavior of concrete slabs-on-ground”, *ACI Mater. J.* **103**:1 (2006), 3–10.
- [Shentu et al. 1997] L. Shentu, D. Jiang, and C. T. T. Hsu, “Load-carrying capacity for concrete slabs on grade”, *J. Struct. Eng. (ASCE)* **123**:1 (1997), 95–103.
- [Silva et al. 2001] R. D. A. Silva, R. A. M. Silveira, and P. B. Gonçalves, “Numerical methods for analysis of plates on tensionless elastic foundations”, *Int. J. Solids Struct.* **38**:10–13 (2001), 2083–2100.
- [Sokól-Supel 1985] J. Sokól-Supel, “Elastoplastic bending of plates resting on elastic subgrade under rotational symmetry conditions”, *J. Struct. Mech.* **13**:3-4 (1985), 323–341.
- [Sokól-Supel 1988] J. Sokól-Supel, “Bending of metallic circular plates resting on elastic subgrade”, *Ing. Arch.* **58** (1988), 185–192.
- [Soutsos et al. 2012] M. N. Soutsos, T. T. Le, and A. P. Lampropoulos, “Flexural performance of fibre reinforced concrete made with steel and synthetic fibres”, *Construction and Building Materials* **36** (2012), 704–710.
- [Tekinalp 1957] B. Tekinalp, “Elastic-plastic bending of a built-in circular plate under a uniformly distributed load”, *J. Mech. Phys. Solids* **5**:2 (1957), 135–142.
- [Timoshenko and Woinowsky-Krieger 1959] S. Timoshenko and S. Woinowsky-Krieger, *Theory of plates and shells*, 2nd ed., McGraw-Hill, New York, 1959.

[Westergaard 1948] H. M. Westergaard, "New formulas for stresses in concrete pavements of airfields", *Trans. ASCE* **113** (1948), 425–444.

Received 11 Dec 2013. Revised 21 Feb 2014. Accepted 10 Mar 2014.

ENRICO RADI: eradi@unimore.it

Dipartimento di Scienze e Metodi dell'Ingegneria, Università di Modena e Reggio Emilia, Via Amendola 2, I-2 42122 Reggio Emilia, Italy

PIETRO DI MAIDA: pietro.dimaida@unimore.it

Dipartimento di Scienze e Metodi dell'Ingegneria, Università di Modena e Reggio Emilia, Via Amendola 2, I-2 42122 Reggio Emilia, Italy

JOURNAL OF MECHANICS OF MATERIALS AND STRUCTURES

msp.org/jomms

Founded by Charles R. Steele and Marie-Louise Steele

EDITORIAL BOARD

ADAIR R. AGUIAR	University of São Paulo at São Carlos, Brazil
KATIA BERTOLDI	Harvard University, USA
DAVIDE BIGONI	University of Trento, Italy
IWONA JASIUK	University of Illinois at Urbana-Champaign, USA
THOMAS J. PENCE	Michigan State University, USA
YASUhide SHINDO	Tohoku University, Japan
DAVID STEIGMANN	University of California at Berkeley

ADVISORY BOARD

J. P. CARTER	University of Sydney, Australia
D. H. HODGES	Georgia Institute of Technology, USA
J. HUTCHINSON	Harvard University, USA
D. PAMPLONA	Universidade Católica do Rio de Janeiro, Brazil
M. B. RUBIN	Technion, Haifa, Israel

PRODUCTION production@msp.org

SILVIO LEVY Scientific Editor

See msp.org/jomms for submission guidelines.

JoMMS (ISSN 1559-3959) at Mathematical Sciences Publishers, 798 Evans Hall #6840, c/o University of California, Berkeley, CA 94720-3840, is published in 10 issues a year. The subscription price for 2014 is US\$555/year for the electronic version, and \$710/year (+\$60, if shipping outside the US) for print and electronic. Subscriptions, requests for back issues, and changes of address should be sent to MSP.

JoMMS peer-review and production is managed by EditFLOW[®] from Mathematical Sciences Publishers.

PUBLISHED BY

 **mathematical sciences publishers**
nonprofit scientific publishing

<http://msp.org/>

© 2014 Mathematical Sciences Publishers

Journal of Mechanics of Materials and Structures

Volume 9, No. 3

May 2014

- B-splines collocation eigenanalysis of 2D acoustic problems**
CHRISTOPHER G. PROVATIDIS 259
- Multi-region Trefftz collocation grains (MTCGs) for modeling piezoelectric composite and porous materials in direct and inverse problems**
PETER L. BISHAY, ABDULLAH ALOTAIBI and SATYA N. ATLURI 287
- Analytical solution for ductile and FRC plates on elastic ground loaded on a small circular area**
ENRICO RADI and PIETRO DI MAIDA 313
- Solution of a receding contact problem using an analytical method and a finite element method**
ERDAL ÖNER, MURAT YAYLACI and AHMET BIRINCI 333
- Sliding of a cup-shaped die on a half-space: influence of thermal relaxation, convection and die temperature**
LOUIS MILTON BROCK 347



1559-3959(2014)9:3;1-7